Characteristics of Station-Derived Convective Cold Pools Over Equatorial Africa

Jannik Hoeller[1,2], Jan O. Haerter[1,2,3,4], Nicolas Da Silva[1]

[1]Integrated Modeling, Leibniz Centre for Tropical Marine Research, Fahrenheitstr. 6, 28359 Bremen, Germany

[2]Niels Bohr Institute, Copenhagen University, Blegdamsvej 17, 2100 Copenhagen, Denmark

[3]Physics and Earth Sciences, Constructor University Bremen, Campus Ring 1, 28759 Bremen, Germany

[4]Department of Physics and Astronomy, University of Potsdam, Karl-Liebknecht-Straße 32, 14476 Potsdam, Germany

Key Points:

- 4289 cold pools are identified across equatorial Africa based on temperature and wind criteria.
- The occurrence and intensity of the observed cold pools are related to low-level moisture conditions and the depth of convection.
- The identified cold pool gust fronts closely correlate with satellite-observed brightness temperature discontinuities.

Corresponding author: Jannik Hoeller, `jannik.hoeller@leibniz-zmt.de`

Abstract

Due to their potential role in organizing tropical mesoscale convective systems, a better understanding of cold pool (CP) dynamics in such regions is critical, particularly over land where the diurnal cycle further concentrates convective activity. Numerical models help disentangle the processes involved but often lack observational benchmark studies. To close this gap, we analyze nearly 43 years of five-minute resolution near-surface timeseries records from twelve automatic weather stations across equatorial Africa. We identify 4289 CPs based on criteria for temperature and wind. The identified CP gust fronts, which exhibit respective median temperature and specific humidity decreases of $5.2\,K$ and $2.8\,g/kg$, closely correlate with satellite-observed brightness temperature discontinuities. Despite weak diurnal variation in precipitation, observed CP occurrence shows a pronounced diurnal cycle with an afternoon peak — a finding we attribute to low-level moisture conditions. Our findings can serve as observational benchmark to improve simulations of CP organization.

Plain Language Summary

Convective cold pools form when rain evaporates underneath thunderstorm clouds. The evaporation causes the air to cool and sink toward the ground, where it is deflected horizontally. Cold pools are thus associated with strong gusty winds, and over tropical land, they can be especially vigorous. Cold pools are also suggested to contribute to the organization of thunderstorm clouds into large clusters of rain-producing areas. The widespread, heavy rainfall can then cause flooding. To better predict such flooding in numerical weather models, having a precise observational basis for cold pool properties is essential — yet currently missing in equatorial Africa. We here provide such an observational benchmark by analyzing thousands of cold pools using timeseries of near-surface temperature, wind, humidity and precipitation. We additionally show that the cold pools can even be detected from satellite data when analyzing abrupt changes in cloud top temperature. Such satellite-based detection could open for cold pool studies across all tropical land areas — of great practical relevance to the prediction of thunderstorm clusters.

1 Introduction

Convective cold pools (CPs) are caused by the evaporation of rainfall beneath deep convective clouds (Zuidema et al., 2017). The resultant denser air volume within the subcloud layer spreads out laterally along the surface and is known to cause a so-called "gust front" along its edges. The gust front features strong horizontal and vertical winds along with moisture and temperature anomalies which together can give rise to additional deep convective events, e.g., under collisions (Purdom, 1976; Feng et al., 2015). CPs are thus important agents in mediating interactions between deep convective cells and thus the self-organization of thunderstorm systems (Simpson, 1980; Tompkins, 2001b; Haerter et al., 2019; Jensen et al., 2021).

Recent idealized cloud-resolving and large-eddy simulations have provided new quantitative and qualitative insight into CP structure and dynamics, such as scaling analysis to obtain a required mesh resolution (Fiévet et al., 2022), the potential origin of moisture rings (Langhans & Romps, 2015; Drager et al., 2020), and insight into interaction mechanisms (Tompkins, 2001a; Torri et al., 2015; Meyer & Haerter, 2020; Haerter et al., 2020). Such simulation studies have also triggered a range of simplified conceptual models, (Böing, 2016; Haerter, 2019; Haerter et al., 2019; Nissen & Haerter, 2021; Niehues et al., 2022), which may help elucidate some of the organizing mechanisms involved. New methods of CP detection in numerical studies have also been developed, which help automatize the tracking of CP gust fronts and their interactions in space and time (Gentine et al., 2016; Torri & Kuang, 2019; Fournier & Haerter, 2019; Henneberg et al., 2020; Hoeller et al., 2022; Hoeller, Fiévet, & Haerter, 2023).

Despite this progress in numerical and theoretical work, direct measurements of CPs are still limited to specific geographic regions, such as the tropical and sub-tropical ocean (Zipser, 1977; Zuidema et al., 2012; Vogel, 2017; Chandra et al., 2018; Vogel et al., 2021), and mid-latitude continental regions in Central Europe (Kirsch et al., 2021; Kruse et al., 2022) or North America (Mueller & Carbone, 1987; Wakimoto, 1982; Engerer et al., 2008; Hitchcock et al., 2019; van den Heever et al., 2021). With a focus on dust storms, in semi-arid tropical regions a CP detection method was suggested based on surface measurements and satellite microwave data (Redl et al., 2015).

The importance of collecting information on CPs and precipitation in deep tropical regions has been pointed out (Adams et al., 2015) but systematic, climatological studies on CPs in such regions are still rare or lacking. This may partially be due to difficult environmental conditions which pose challenging demands on equipment and maintenance (Parker et al., 2008). Also the availability of funds may hinder systematic long-term campaigns in some regions. A notable exception is the trans-African hydro-meteorological observatory (TAHMO) which offers a promising network of station measurements in many sub-Saharan African countries (van de Giesen et al., 2014). Using a range of stations from the TAHMO network, we here present a climatology of CP measurements for equatorial Africa and compare findings to previous work in other geographic regions.

2 Data

2.1 Station data

We utilize data from twelve ATMOS41 automatic weather stations (AWS) in equatorial Africa (Fig. 1), operated by TAHMO (TAHMO, 2023). The stations are situated in Cameroon, the Democratic Republic of the Congo (DR Congo), Nigeria, and Uganda. In order to investigate the influence of regional climatic differences on CPs, we group stations according to their respective deployment countries in the following analysis.

The AWS provide data at a temporal resolution of five minutes. All stations are installed at an approximate height of two meters above the surface. For our analysis, we employ the station records of precipitation, atmospheric pressure, air temperature, relative humidity, and wind gust speed. To derive the wind gust speed, the ATMOS41 measures the instantaneous wind speed every ten seconds and outputs the maximum instantaneous wind speed value within the corresponding five-minute interval as wind gust speed. If an instantaneous wind speed is larger than eight times the running average of the previous ten instantaneous measurements, the measurement is rejected. While this method may prevent spurious spikes in the wind record under normal conditions, it can cause missing wind data in cases of large and sudden wind changes. Given the frequent occurrence of such strong wind variations associated with CP gust fronts, approximately 22% of all identified CPs have an incomplete wind record.

We analyze the data recorded by the stations from January 1, 2019, to September 30, 2023. As not all stations were operational throughout the entire period, we limit our analysis for each station to days with complete air temperature record. Additionally, we require the air temperature to be recorded for a minimum of ten consecutive minutes from the previous day and for the subsequent 120 minutes on the following day. The resulting number of analysis days per station is indicated in Fig. 1. In total, we analyzed 15602 days and thus nearly 43 years of station data.

Based on the station-measured variables, we additionally compute both mixing ratio, r and saturated mixing ratio, r_{sat} (see Text S1), and derive the mixing ratio deficit, $r_D \equiv r_{sat} - r$ and the specific humidity, $q \equiv r/(1 + r)$.
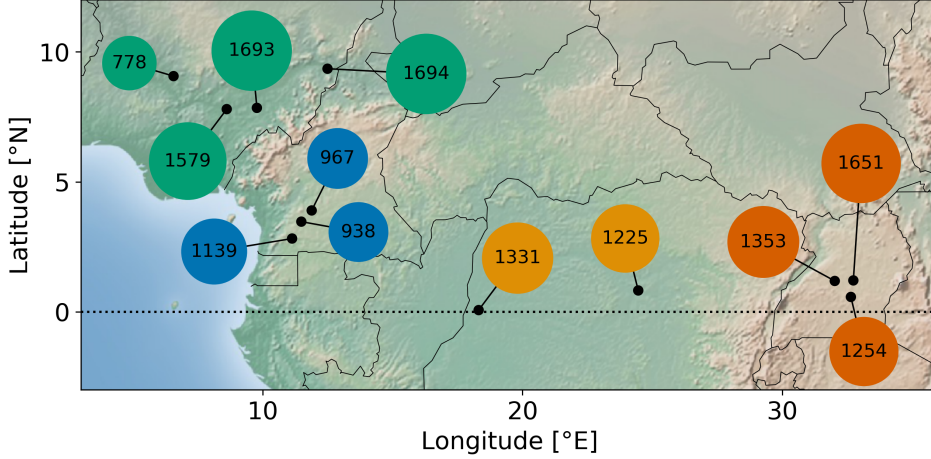
Figure 1: **Employed weather station data.** Map of equatorial Africa with station locations (filled black circles) utilized in this study. Numbers represent available days of station data with a complete record of air temperature, T. The stations are grouped into four regions denoted by the colored circles: Cameroon (blue), Democratic Republic of the Congo (yellow), Nigeria (green), Uganda (red). The area of colored circles is proportional to the available days of station data.

2.2 Satellite data

Apart from the station data, we utilize infrared brightness temperature measurements which we derive from satellite-measured effective radiances. The radiances are extracted from Meteosat Second Generation (MSG) 0° products provided by the European Organisation for the Exploitation of Meteorological Satellites (EUMETSAT) (EUMETSAT, 2023). The data has a baseline repeat cycle of $15\,min$ and a spatial resolution of $3\,km$ in the sub-satellite point. To convert the radiances to brightness temperatures we employ equation 5.3 and the corresponding regression coefficients of EUMETSAT (2012).

3 Methods

3.1 Cold Pool Detection Algorithm

(i) Temperature criterion. A potential CP event is detected at a given time t if three conditions apply: similar to Kirsch et al. (2021) we require a substantial temperature decrease $\Delta T \leq -2\,K$, within the $20\,min$ window from $t - 5\,min$ to $t + 15\,min$. Additionally, we require the decrease of ΔT to be monotonic and $T(t) - T(t - 5\,min) \leq 0.5\,K$.

(ii) Wind criterion. To verify detected potential CP events, we adapt the wind criterion introduced by Kruse et al. (2022). For this purpose, we compute the wind gust anomaly for each time t as

$$\Delta u_g(t) \equiv u_g(t) - \overline{u}_g(t)\,, \tag{1}$$

where u_g is the wind gust speed and $\overline{u}_g$ its centered 2-hour running mean, i.e., the mean value of the 25 wind gust speeds recorded during the the corresponding 2-hour window.

For a potential CP event at time t we identify the maximum wind gust anomaly, Δu_g^{max}, between $t - 20\,min$ and $t + 40\,min$. We consider it as CP event if

$$\Delta u_g^{max} \geq \overline{\Delta u}_g(t) + 3\,\sigma_{\Delta u_g}(t)\,, \tag{2}$$

¹³¹ with the centered 24-hour running mean of the wind gust anomaly, $\overline{\Delta u_g}$, and the cor-
¹³² responding 24-hour running standard deviation, $\sigma_{\Delta u_g}$.

¹³³ As the CP onset is defined based on the temperature criterion, we also search for
¹³⁴ associated wind gusts in a $20\,min$ time window before CP onset. We choose $20\,min$ rather
¹³⁵ than the $10\,min$ used by Kruse et al. (2022) since our temperature criterion involves a
¹³⁶ minimum decrease of $-0.5\,K$ within $5\,min$ to define the onset of potential CPs and might
¹³⁷ thus delay the onset in comparison to Kruse et al. (2022). The $40\,min$ time window af-
¹³⁸ ter CP onset allows significant wind offsets while ensuring a temporal relation between
¹³⁹ ΔT and Δu_g^{max}.

In case of missing wind gust anomalies between $t-20\,min$ and $t+40\,min$, we iden-
tify the maximum wind gust, u_g^{max} within this time window rather than Δu_g^{max} and con-
sider the event a CP if

$$u_g^{max} \geq \overline{u}_g(t - 80\,min) + 2\,\sigma_{u_g}(t - 80\,min). \tag{3}$$

¹⁴⁰ By evaluating the centered 2-hour running mean $\overline{u}_g$ and the corresponding stan-
¹⁴¹ dard deviation, σ_{u_g}, $80\,min$ before CP onset, we keep again a $20\,min$ offset between CP
¹⁴² onset and the 2-hour time window of the reference values. If no wind gust data has been
¹⁴³ recorded between $t - 20\,min$ and $t + 40\,min$, or if the reference values $\overline{u}_g(t - 80\,min)$
¹⁴⁴ and $\overline{u}_g(t-80\,min)$ could not be computed due to missing data, we consider the event
¹⁴⁵ as "no CP."

¹⁴⁶ Differing from Kruse et al. (2022), we evaluate the wind criterion based on wind
¹⁴⁷ gust rather than wind speed. Since we work with station data with a temporal resolu-
¹⁴⁸ tion of $5\,min$ in contrast to $1\,min$ in (Kruse et al., 2022), we find wind gust a better in-
¹⁴⁹ dicator for CP gust fronts than wind speed.

¹⁵⁰ **(iii) Duplicate detection check.** Often, a CP fulfills the defined criteria (i) and (ii)
¹⁵¹ not only at time t, but also at subsequent time steps. Depending on the evolution of tem-
¹⁵² perature and wind gust behind the CP gust front, time steps in which the criteria are
¹⁵³ met can even be separated from each other by time steps in which the criteria are not
¹⁵⁴ met. In order to avoid duplicate detection of a given CP, we drop detected CP events
¹⁵⁵ if at least one other CP event was detected within $20\,min$ before that particular event.
¹⁵⁶ Given the variety of environmental conditions under which we observe CPs at our sta-
¹⁵⁷ tion locations, we find this definition to be more permissive than the absolute $60\,min$ time
¹⁵⁸ window after detected temperature decreases, within which Kirsch et al. (2021) consider
¹⁵⁹ any detected decrease as part of the same event.

¹⁶⁰ ### 3.2 Determination of Cold Pool Anomalies

¹⁶¹ We analyze the effects of a detected CP with respect to different station-measured
¹⁶² meteorological variables by considering a time window relative to CP onset, t_0, from t_0-
¹⁶³ $40\,min$ to $t_0+120\,min$. Within this time window, we evaluate the CP associated anoma-
¹⁶⁴ lies $y'(t) \equiv y(t) - y_{ref}$ for a meteorological variable y based on an unperturbed refer-
¹⁶⁵ ence state y_{ref}, which we define as the temporal mean of instantaneous measurements
¹⁶⁶ in a time interval before CP onset. Since the onset is defined based on the temperature
¹⁶⁷ drop and thus could be different for other variables, we choose the time interval from t_0-
¹⁶⁸ $40\,min$ to $t_0-20\,min$ to keep a sufficient margin of $20\,min$ to the CP onset while pre-
¹⁶⁹ serving the required temporal proximity. To minimize any distortion of the reference state
¹⁷⁰ through the diurnal cycle, we deviate from this definition only for temperature anoma-
¹⁷¹ lies and follow the approach of the refined temperature drop from Kruse et al. (2022)
¹⁷² instead, i.e., we consider the maximum temperature of the two measurements in the $10\,min$
¹⁷³ time window preceding the CP onset as unperturbed reference temperature.

¹⁷⁴ Due to the coarser temporal resolution, we extend the time window in which we
¹⁷⁵ analyze the anomalies before CP onset to $60\,min$ for satellite-measured $10.8\,\mu m$ bright-

ness temperatures, $BT_{10.8}$, and define the reference brightness temperature, $BT_{10.8}^{ref}$, as the mean of the three observations in the time interval from $t_0 - 60\,min$ to $t_0 - 30\,min$. As there might not be a brightness temperature observation at the station-derived CP onset, t_0, we define the closest satellite time step as $\hat{t}_0$ and measure the CP time relative to it. The brightness temperature anomalies, $BT'_{10.8}$, are then computed analogously to those for station-measured variables. Moreover, to further investigate the space-borne CP signature, we additionally determine the temporal change of $BT'_{10.8}$, as $\Delta BT'_{10.8}(t) = BT'_{10.8}(t) - BT'_{10.8}(t - 15\,min)$.

4 Results

4.1 Seasonal and Diurnal Cycle of Observed Cold Pools

First, we derive the seasonal and diurnal cycles of CPs in the different sub-regions (Fig. 1) and relate them with precipitation, convection depth and moisture conditions (Fig. 2). With about 0.3–0.6 CPs per day in the high seasons (Fig. 2a, Table S2), equatorial Africa is a region with particular CP abundance compared to previous climatologies in other continental regions (Redl et al., 2015; Kirsch et al., 2021; Kruse et al., 2022). In every sub-region, the number of CPs peaks twice during the course of the year with a first maximum between March and May and a second maximum between September and October. The bi-modality in the annual cycle of CPs largely corresponds to the latitudinal migration of the Inter-Tropical Convergence Zone (ITCZ) which is reflected in the precipitation seasonal cycles (Fig. 2c). However, we note that precipitation may not explain all the features of the annual cycle of CPs and the differences between sub-regions. For instance, Nigeria presents a single precipitation peak in September whereas the occurrence of CPs peaks in both May and September. There, the strong CP activity during May may be related to the combination of deeper convection (Fig. 2e) fed by high equivalent potential temperatures (θ_E; Fig. S1) and of higher low-level water vapor mixing ratio deficit (r_D; Fig. 2g) boosting rain evaporation. We also note that Uganda receives the least precipitation among sub-regions while experiencing the most of CPs during the year. We attribute the larger number of CPs in Uganda to generally drier conditions at low levels (Fig. 2g).

The diurnal cycle of CPs strongly peaks between 15 LT and 18 LT in most of the regions with the exception of Nigeria where the peak is reached between 18 LT and 21 LT (Fig. 2b). The high CP activity during the afternoon can be directly related to the afternoon peak in (deep) convection, highlighted by maxima in precipitation (Fig. 2d) and lower brightness temperatures (Fig. 2f). Consistently with earlier studies (Zhang et al., 2016; Camberlin et al., 2018; Andrews et al., 2023), precipitation shows secondary nocturnal peaks in Uganda and Congo, and remains high during the night in Nigeria, whereas the proportion of CPs displays local minima during these hours. This mismatch between precipitation and CPs is likely to be related to both the decline of convection during the night (leading to weaker rainfall intensities and downdrafts) and to moister conditions at the surface (reducing rainfall evaporative cooling; Fig. 2h) which both inhibit CP formation (Zuidema et al., 2017).

4.2 Observed Cold Pool Characteristics

We further characterize equatorial African CPs by examining their related temperature and moisture anomalies (defined in Sec. 3.2). On average, a CP in equatorial Africa is accompanied by a $5\,K$ drop in temperature (compared to $3\,K$ in Germany; Kirsch et al. (2021)) occurring in about 30 minutes, with little variability among sub-regions (Fig. 3a, Table S2). Different from Kirsch et al. (2021) over Germany, we generally observe a decrease in specific humidity after the passage of CPs over equatorial Africa (Fig. 3d). Interestingly, we find that the magnitude of this decrease is smaller in the elevated (Table S1) stations of Uganda ($-1\,g/kg$) characterized by less deep convection (Fig. 2e,f)
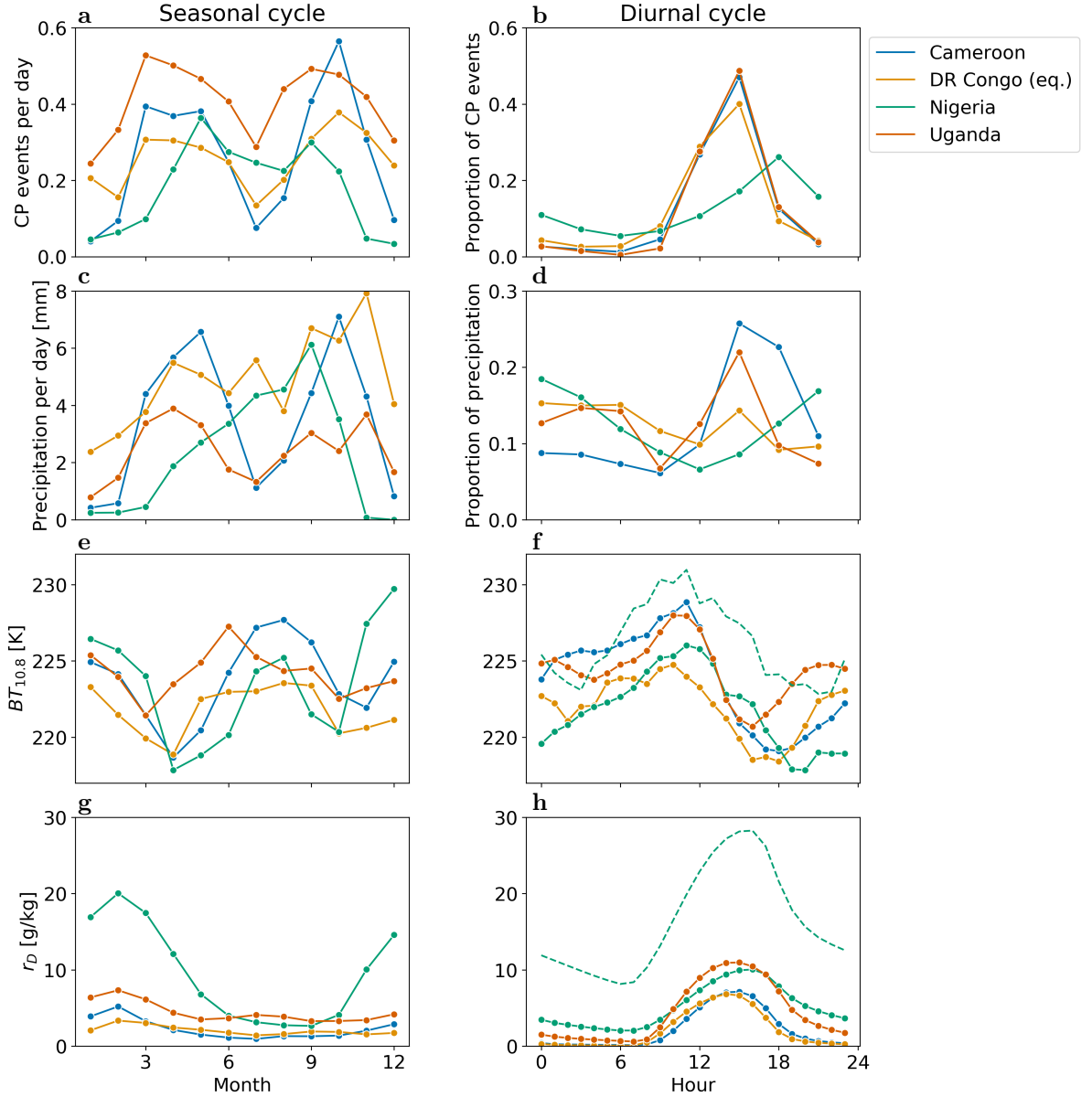
Figure 2: **Observed seasonal and diurnal cycles. a**, Mean number of daily cold pool (CP) events for each month. Lines interpolate linearly between markers to facilitate the interpretation; colors indicate different regions. The number of CP events is normalized based on the number of analyzed days per month and region. **b**, Proportion of CP events at different times of the day. Each marker represents the proportion of CP events observed within a given 3-hour time interval, starting with the interval [0,3) for the marker at 0 LT. Lines and colors analogous to (a). **c**, Analogous to (a) but for precipitation. **d**, Analogous to (b) but for precipitation. **e**, Mean $10.8\,\mu m$ brightness temperature, $BT_{10.8}$, of deep clouds ($BT_{10.8} \leq 240\,K$) for each month. Lines and colors analogous to (a). **f**, Mean $BT_{10.8}$ of deep clouds at different times of the day. Intervals, lines and colors analogous to (b). The two lines for Nigeria represent rainy months (Apr–Oct, solid line with markers) and dry months (Nov–Mar, dashed). **g**, Analogous to (e) but for mean mixing ratio deficit, r_D. **h**, Analogous to (f) but for mean r_D.

and drier low-level environments (Fig. 2g,h) compared to the other sub-regions (about $-3\,g/kg$). Less deep convection is likely to be associated with less elevated (relative to the surface level) convective downdrafts (Zuidema et al., 2017) importing less upper-level dry air to the surface, which combined with enhanced rain evaporation due to drier environments, may explain the reduced decline in specific humidity over Uganda. When considering the 25% driest (moistest) low-level pre-CP environments, we further evidence the large impact of moisture conditions, and thus of rain evaporation, on CP temperature and moisture anomalies in all sub-regions (Fig. 2b,c,e,f). Indeed, we find CP anomalies that are on average $3\,K$ cooler and $2\,g/kg$ moister in the driest pre-CP conditions than in the moistest pre-CP conditions. We note weak maxima in specific humidity occurring few minutes after the CP onset (so-called moisture rings) over Cameroon, Uganda and Congo for the driest pre-CP environments. Finally, the temporal evolutions of r_D (Fig. 3g,h,i) reveal that in the driest environments, rain evaporation is not sufficient to saturate the low-level air (similar to Germany; Kirsch et al. (2021)).
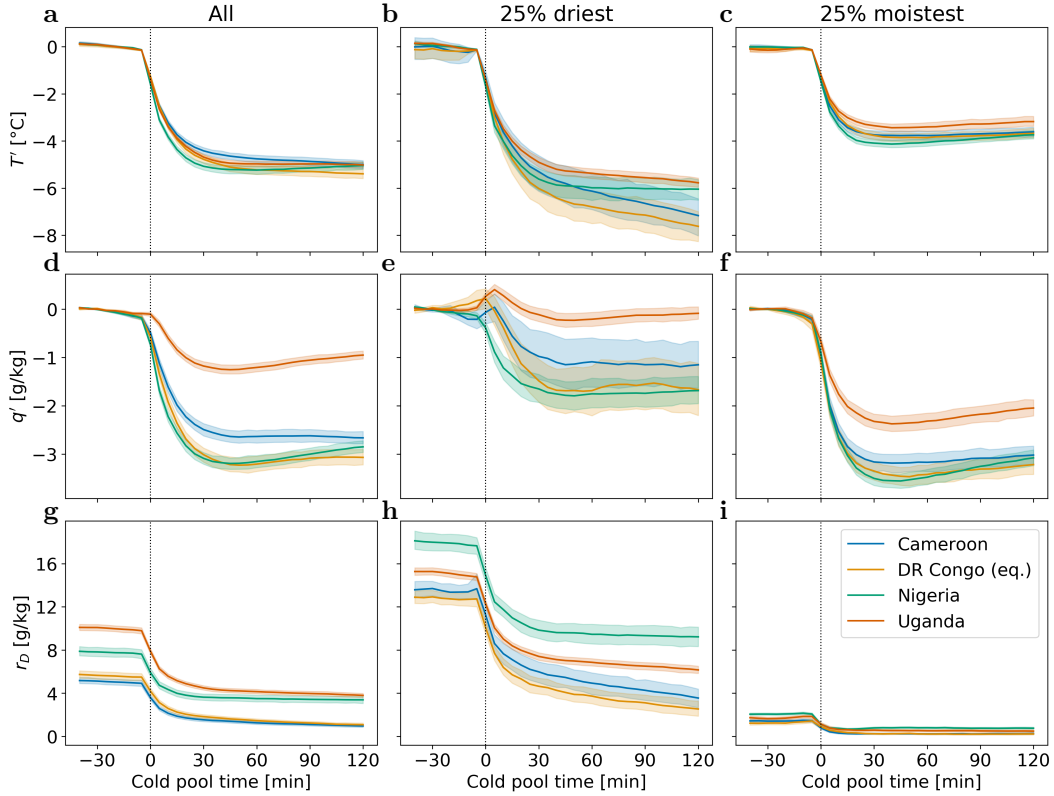

Figure 3: **Station-derived cold pool (CP) properties relative to CP onset, t_0.** **a**, Mean temperature anomalies, T', for different regions; shading indicates the 95% confidence interval. **b**, Analogous to (a) but for the 25% driest CPs of each region w.r.t. the reference mixing ratio deficit, r_D^{ref}, prior to t_0. **c**, Analogous to (b) but for the 25% moistest CPs. **d–f**, Analogous to (a)–(c) but for mean specific humidity anomalies, q'. **g– i**, Analogous to (a)–(c) but for mean mixing ratio deficits, r_D. Note that only timeseries of CPs, where t_0 is more than 120 minutes apart from other CP onsets, are included in the analysis.

Moving to CP cloud characteristics, we find that 92% (Nigeria) to 100% (Congo) of CP gust fronts are accompanied by shallow or deep convective clouds (Fig. S2a). More specifically, a CP is generally accompanied by a strong (reaching $30\,K$ in Cameroon) decrease in $BT_{10.8}$ (Fig. 4a). The $BT_{10.8}$ minimum is typically reached 30–45 minutes af-

ter CP onset. While this minimum is delayed w.r.t. the CP onset, we find a minimum of the time derivative of $BT'_{10.8}$ synchronized with the CP onset in all sub-regions (Fig. 4b). This observation suggests that CPs in equatorial Africa, and potentially other regions, might be detectable from space-borne satellite data.
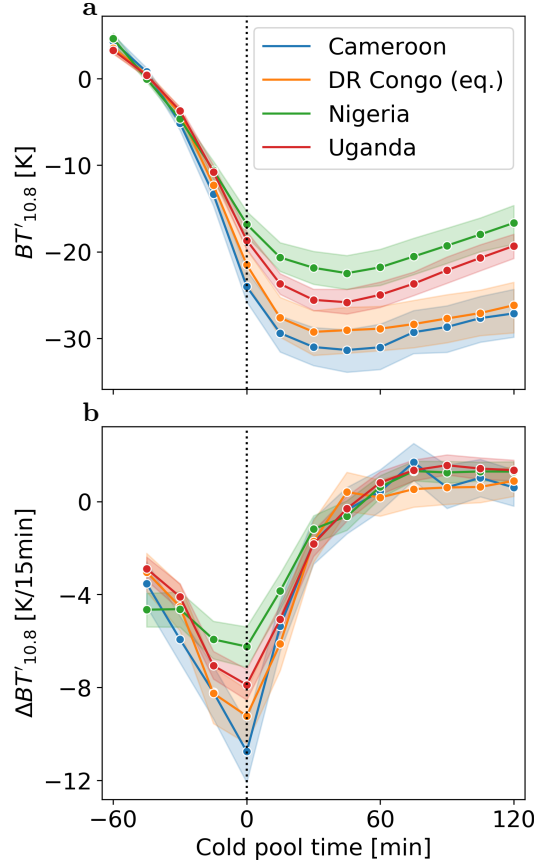

Figure 4: **Space-borne signatures of cold pools (CPs) relative to CP onset, $\hat{t}_0$. a**, Mean $10.8\mu m$ brightness temperature anomalies, $BT'_{10.8}$, of station-derived CPs for different regions; shading indicates the 95% confidence interval. **b**, Analogous to (a) but for the corresponding derivative $\Delta BT'_{10.8}$.

4.3 Cold Pool Examples With Deep and Shallow Convection

We now turn to two contrasting examples of observed CPs (Fig. 5). The two station locations at which the CPs were detected are indicated in Fig. 5a).

The first CP (Fig. 5; left column) was detected in DR Congo at station TA673 on November 28, 2021, at 13:40 UTC. The CP was associated with a mesoscale convective system, visible in the satellite-derived $10.8\,\mu m$ brightness temperature image at 13:45 UTC (Fig. 5b). The corresponding brightness temperature timeseries of different satellite channels at the station are depicted in Fig. 5d). All channels show a significant brightness temperature decrease around CP onset, with a maximum decrease rate right at the onset. Between 12:30 and 14:45 UTC, the brightness temperature dropped by $85\,K$ in the $10.8\,\mu m$ channel and then slowly increased again. The station record (Fig. 5f) further reveals a massive air temperature drop of $9.6\,K$ between 13:40 and 14:00 UTC, accompanied by increased wind gust speeds of up to $6.5\,m/s$. By 14:00 UTC, when the tem-

perature stabilized again, the air became fully saturated. Five minutes later, the rain-fall intensity peaked at approximately $65 \, mm/h$.

The second CP (Fig. 5; right column) was detected in Uganda at station TA222 on July 2, 2021, at 12:05 UTC. During the time it was detected, the CP featured arc-shaped shallow convection at the gust front, distinctly separated from the parent con-vection by clear skies (Fig. 5c). The corresponding brightness temperature timeseries at the station (Fig. 5e) confirm the passage of low-level clouds right at the time of the station-derived CP onset. Around the CP onset, no rainfall was measured at the station (Fig. 5g). This time, the observed wind gust speeds increase approximately 5–10 minutes before the drop in air temperature and reach a peak value of $10 \, m/s$ at CP onset.

5 Summary and Discussion

The present study provides multi-year statistics of cold pool characteristics in equa-torial Africa, based on five-minute near-surface weather data. Using detection methods similar to those in previous studies focused on mid-latitude continental regions, key find-ings include that temperature drops upon gust front passage often exceed $5 \, K$ and spe-cific humidities typically decrease by more than $3 \, g/kg$. Weak moisture rings can only be identified for the driest cold pools in some of the regions — in agreement with Kruse et al. (2022) for data in the Netherlands where moisture rings were generally not detected.

Seasonally, the rate of cold pool occurrence roughly follows precipitation statistics. Yet, diurnally, the fact that the nocturnal boundary layer is often close to saturation may focus the diurnal cycle of cold pool occurrence on the drier late afternoon times. This may have important implications for thunderstorm organization through cold pool ac-tivity: the limited time window where cold pools actually occur during the day means that self-organization may be limited to relatively short periods of the day. One could speculate that it is the lack of cold pool activity that limits the duration of mesoscale convective systems, often less than 12 hours, rather than the precipitation itself (which is more spread out over the day). Future studies should analyze if deep convection is more scattered during the nocturnal periods when fewer cold pools occur. Comparisons with oceanic cold pools and their organizational effects, which tend to be weaker (Zuidema et al., 2017), would be useful.

Our cold pool detection algorithm can be adapted to other regions, provided that there are in-situ weather stations measuring surface wind and temperature with at least a 5-minute temporal resolution. However, in-situ weather stations meeting this require-ment are still limited in the tropics, whereas cold pools are abundant. Encouragingly, our findings may have implications for satellite-based cold pool detection: we show that the gust front passage clearly correlates with discontinuities in satellite-derived bright-ness temperature. We generally observe a significant decrease in brightness temperatures around the time of the gust front passage, with maximum decrease rates at the station-derived cold pool onset. Our findings thus suggest that cold pools in equatorial Africa, and potentially other regions, could be directly detectable from geostationary satellite data on a continental scale. Even in cases where not all parts of a cold pool gust front exhibit brightness temperature drops (Fig. S2b), neural networks, such as those devel-oped by Hoeller, Fiévet, and Haerter (2023), may still possess the capability to detect the overall two-dimensional pattern and accurately track the gust front.
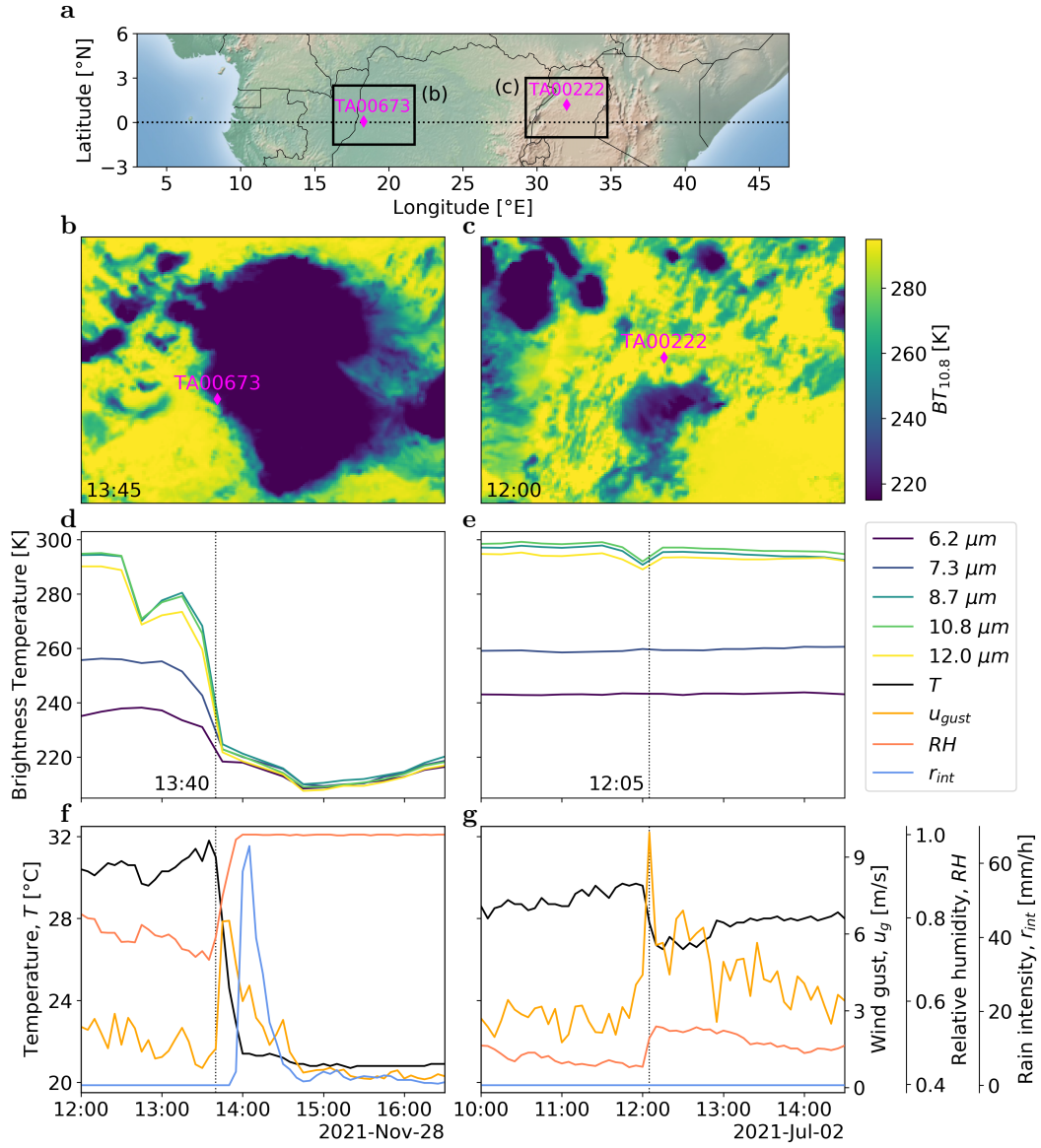
Figure 5: **Cold pool (CP) case studies. a**, Map displaying the locations of the stations utilized in the two case studies. Rectangles indicate the regions depicted in (b) and (c). **b**, Satellite-derived $10.8\mu m$ brightness temperatures, $BT_{10.8}$, in the vicinity of station TA00673 on November 28, 2021, at 13:45, close to a station-derived CP onset at 13:40. **c**, Analogous to (b) but for station TA00222 on July 2, 2021, at 12:00 and a CP onset at 12:05. **d**, Timeseries of satellite-derived brightness temperatures at station TA673 during the CP event visualized in (b). **e**, Analogous to (d) but for the CP event at station TA222 visualized in (c). **f-g**, Analogous to (d-e) but for different near-surface observations.

Data Availability Statement

Conflicts of Interest Statement

The authors have no conflicts of interest to declare.

Acknowledgments

References

Adams, D. K., Fernandes, R. M., Holub, K. L., Gutman, S. I., Barbosa, H. M., Machado, L. A., ... others (2015). The amazon dense gnss meteorological network: A new approach for examining water vapor and deep convection interactions in the tropics. *Bulletin of the American Meteorological Society*, *96*(12), 2151–2165.

Andrews, P. C., Cook, K. H., & Vizy, E. K. (2023). Mesoscale convective systems in the congo basin: seasonality, regionality, and diurnal cycles. *Climate Dynamics*, 1–22. doi: 10.1007/s00382-023-06903-7

Böing, S. J. (2016). An object-based model for convective cold pool dynamics. *Mathematics of Climate and Weather Forecasting*, *2*(1).

Camberlin, P., Gitau, W., Planchon, O., Dubreuil, V., Funatsu, B. M., & Philippon, N. (2018). Major role of water bodies on diurnal precipitation regimes in eastern africa. *International Journal of Climatology*, *38*(2), 613-629. Retrieved from https://rmets.onlinelibrary.wiley.com/doi/abs/10.1002/joc.5197 doi: https://doi.org/10.1002/joc.5197

Caswell, T. A., Droettboom, M., Lee, A., de Andrade, E. S., Hoffmann, T., Klymak, J., ... Ivanov, P. (2022). *matplotlib/matplotlib: Release (version 3.5.2) [software]*. Zenodo. Retrieved from https://doi.org/10.5281/zenodo.6513224 doi: 10.5281/zenodo.6513224

Chandra, A. S., Zuidema, P., Krueger, S., Kochanski, A., de Szoeke, S. P., & Zhang, J. (2018). Moisture distributions in tropical cold pools from equatorial indian ocean observations and cloud-resolving simulations. *Journal of Geophysical Research: Atmospheres*, *123*(20), 11–445.

Drager, A. J., Grant, L. D., & van den Heever, S. C. (2020). Cold pool responses to changes in soil moisture. *Journal of Advances in Modeling Earth Systems*,

12(8), e2019MS001922.

Engerer, N. A., Stensrud, D. J., & Coniglio, M. C. (2008). Surface characteristics of observed cold pools. *Monthly Weather Review*, *136*(12), 4839–4849.

EUMETSAT. (2012). *The conversion from effective radiances to equivalent brightness temperatures (version 1).* Retrieved from `https://www-cdn.eumetsat.int/files/2020-04/pdf_effect_rad_to_brightness.pdf`

EUMETSAT. (2023). *Meteosat second generation (msg) high rate seviri level 1.5 image data - 0 degree [dataset].* Retrieved from `https://navigator.eumetsat.int/product/EO:EUM:DAT:MSG:HRSEVIRI`

Feng, Z., Hagos, S., Rowe, A. K., Burleyson, C. D., Martini, M. N., & de Szoeke, S. P. (2015). Mechanisms of convective cloud organization by cold pools over tropical warm ocean during the amie/dynamo field campaign. *Journal of Advances in Modeling Earth Systems*, *7*(2), 357–381.

Fiévet, R., Meyer, B., & Haerter, J. O. (2022). On the sensitivity of convective cold pools to mesh resolution. *Earth and Space Science Open Archive*, 24. Retrieved from `https://doi.org/10.1002/essoar.10512297.1` doi: 10.1002/essoar.10512297.1

Fournier, M. B., & Haerter, J. O. (2019). Tracking the gust fronts of convective cold pools. *Journal of Geophysical Research: Atmospheres*, *124*(21), 11103–11117.

Gentine, P., Garelli, A., Park, S., Nie, J., Torri, G., & Kuang, Z. (2016). Role of surface heat fluxes underneath cold pools. *Geophys. Res. Lett.*, *43*, 874-883. doi: 10.1002/2015gl067262

Haerter, J. O. (2019). Convective self-aggregation as a cold pool-driven critical phenomenon. *Geophysical Research Letters*, *46*(7), 4017–4028. doi: https://doi.org/10.1029/2018GL081817

Haerter, J. O., Böing, S. J., Henneberg, O., & Nissen, S. B. (2019). Circling in on convective organization. *Geophysical Research Letters*, *46*(12), 7024–7034. doi: https://doi.org/10.1029/2019GL082092

Haerter, J. O., Meyer, B., & Nissen, S. B. (2020). Diurnal self-aggregation. *npj Climate and Atmospheric Science*, *3*. doi: 10.1038/s41612-020-00132-z

Henneberg, O., Meyer, B., & Haerter, J. O. (2020). Particle-based tracking of cold pool gust fronts. *J. Adv. Model. Earth Syst.*, *12*. doi: 10.1029/2019ms001910

Hitchcock, S. M., Schumacher, R. S., Herman, G. R., Coniglio, M. C., Parker, M. D., & Ziegler, C. L. (2019). Evolution of pre-and postconvective environmental profiles from mesoscale convective systems during pecan. *Monthly Weather Review*, *147*(7), 2329–2354.

Hoeller, J., Fiévet, R., & Haerter, J. O. (2022). U-net segmentation for the detection of convective cold pools from cloud and rainfall fields. *Authorea Preprints*.

Hoeller, J., Fiévet, R., & Haerter, J. O. (2023). Detecting cold pool family trees in convection resolving simulations. *Authorea Preprints*.

Hoeller, J., Haerter, J. O., & Silva, N. D. (2023). *Identification algorithm for cold pool gust fronts in weather station data from equatorial africa (version 1.0) [software & dataset].* Zenodo. Retrieved from `https://doi.org/10.5281/zenodo.10117789` doi: 10.5281/zenodo.10117789

Hunter, J. D. (2007). Matplotlib: A 2d graphics environment [software]. *Computing in Science & Engineering*, *9*(3), 90–95. doi: 10.1109/MCSE.2007.55

Jensen, G. G., Fiévet, R., & Haerter, J. O. (2021). The diurnal path to persistent convective self-aggregation. *arXiv preprint arXiv:2104.01132*.

Kirsch, B., Ament, F., & Hohenegger, C. (2021). Convective cold pools in long-term boundary layer mast observations. *Monthly Weather Review*, *149*(3), 811–820.

Kruse, I. L., Haerter, J. O., & Meyer, B. (2022). Cold pools over the netherlands: A statistical study from tower and radar observations. *Quarterly Journal of the Royal Meteorological Society*, *148*(743), 711–726.

Langhans, W., & Romps, D. M. (2015). The origin of water vapor rings in tropical oceanic cold pools. *Geophysical Research Letters*, *42*(18), 7825–7834.

Meyer, B., & Haerter, J. O.   (2020, 11).   Mechanical forcing of convection by cold pools: Collisions and energy scaling.   *J. Adv. Model. Earth Syst.*, *12*(11), n/a–n/a. Retrieved from https://doi.org/10.1029/2020MS002281   doi: 10.1029/2020MS002281

Mueller, C. K., & Carbone, R. E.   (1987).   Dynamics of a thunderstorm outflow.   *Journal of the Atmospheric sciences*, *44*(15), 1879–1898.

Niehues, J., Jensen, G. G., & Haerter, J. O. (2022). Self-organized quantization and oscillations on continuous fixed-energy sandpiles.   *Physical Review E*, *105*(3), 034314.

Nissen, S. B., & Haerter, J. O.   (2021).   Circling in on convective self-aggregation.   *Journal of Geophysical Research: Atmospheres*, *126*(20), e2021JD035331.

Parker, D. J., Fink, A., Janicot, S., Ngamini, J.-B., Douglas, M., Afiesimama, E., ... others   (2008).   The amma radiosonde program and its implications for the future of atmospheric monitoring over africa.   *Bulletin of the American Meteorological Society*, *89*(7), 1015–1028.

Purdom, J. F.   (1976).   Some uses of high-resolution goes imagery in the mesoscale forecasting of convection and its behavior.   *Monthly Weather Review*, *104*(12), 1474–1483.

Redl, R., Fink, A. H., & Knippertz, P.   (2015).   An objective detection method for convective cold pool events and its application to northern africa.   *Monthly Weather Review*, *143*(12), 5055–5072.

Simpson, J.   (1980).   Downdrafts as linkages in dynamic cumulus seeding effects.   *Journal of Applied Meteorology*, *19*(4), 477–487.

TAHMO.   (2023).   *Trans-african hydro-meteorological observatory (tahmo) weather station data [dataset].* Retrieved from https://tahmo.org/climate-data/

Tompkins, A. M.   (2001a).   Organization of tropical convection in low vertical wind shears: The role of cold pools.   *Journal of the Atmospheric Sciences*, *58*, 1650-1672. doi: 10.1175/1520-0469(2001)058<1650:ootcil>2.0.co;2

Tompkins, A. M.   (2001b).   Organization of tropical convection in low vertical wind shears: The role of water vapor.   *Journal of the Atmospheric Sciences*, *58*(6), 529–545.

Torri, G., & Kuang, Z.   (2019).   On cold pool collisions in tropical boundary layers.   *Geophys. Res. Lett.*, *46*, 399-407. doi: 10.1029/2018gl080501

Torri, G., Kuang, Z., & Tian, Y.   (2015).   Mechanisms for convection triggering by cold pools. *Geophysical Research Letters*, *42*(6), 1943–1950.

van de Giesen, N., Hut, R., & Selker, J.   (2014).   The trans-african hydro-meteorological observatory (tahmo).   *Wiley Interdisciplinary Reviews: Water*, *1*(4), 341–348.

van den Heever, S. C., Grant, L. D., Freeman, S. W., Marinescu, P. J., Barnum, J., Bukowski, J., ... others (2021). The colorado state university convective cloud outflows and updrafts experiment (c 3 loud-ex).   *Bulletin of the American Meteorological Society*, *102*(7), E1283–E1305.

Vogel, R.   (2017).   *The influence of precipitation and convective organization on the structure of the trades* (Unpublished doctoral dissertation).   Universität Hamburg Hamburg.

Vogel, R., Konow, H., Schulz, H., & Zuidema, P.   (2021).   A climatology of trade-wind cumulus cold pools and their link to mesoscale cloud organization. *Atmospheric Chemistry and Physics*, *21*(21), 16609–16630.

Wakimoto, R. M.   (1982).   The life cycle of thunderstorm gust fronts as viewed with doppler radar and rawinsonde data.   *Monthly weather review*, *110*(8), 1060–1082.

Waskom, M. L.   (2021).   seaborn: statistical data visualization [software].   *Journal of Open Source Software*, *6*(60), 3021.   Retrieved from https://doi.org/10.21105/joss.03021   doi: 10.21105/joss.03021

Zhang, G., Cook, K. H., & Vizy, E. K.   (2016).   The diurnal cycle of warm season

rainfall over west africa. part i: Observational analysis.   *Journal of Climate*, *29*(23), 8423 - 8437. doi: 10.1175/JCLI-D-15-0874.1

Zipser, E. (1977). Mesoscale and convective–scale downdrafts as distinct components of squall-line structure. *Monthly Weather Review*, *105*(12), 1568–1589.

Zuidema, P., Li, Z., Hill, R. J., Bariteau, L., Rilling, B., Fairall, C., . . . Hare, J. (2012).   On trade wind cumulus cold pools.   *Journal of the Atmospheric Sciences*, *69*(1), 258–280.

Zuidema, P., Torri, G., Muller, C., & Chandra, A. (2017). A survey of precipitation-induced atmospheric cold pools over oceans and their interactions with the larger-scale environment. *Surveys in Geophysics*, 1–23.

References From the Supporting Information

Bolton, D. (1980). The computation of equivalent potential temperature. Monthly weather review , 108 (7), 1046–1053.

Wallace, J. M., & Hobbs, P. V. (2006). Atmospheric science: an introductory survey (Vol. 92). Elsevier.